The Hydrogen-Bonding Structure in Parallel-Stranded Duplex DNA Is Reverse Watson–Crick[†]

C. Otto,[‡,§] G. A. Thomas,[§] K. Rippe,[∥] T. M. Jovin,[∥] and W. L. Peticolas[*,§]

Department of Chemistry, University of Oregon, Eugene, Oregon 97403, and Department of Molecular Biology, The Max Planck Institute for Biophysical Chemistry, Postfach 2841, D-3400 Göttingen, FRG

Received June 13, 1990; Revised Manuscript Received December 3, 1990

ABSTRACT: Raman spectra of the parallel-stranded duplex formed from the deoxyoligonucleotides 5′-d-[(A)$_{10}$TAATTTTAAATATTT]-3′ (D1) and 5′-d[(T)$_{10}$ATTAAAATTTATAAA]-3′ (D2) in H$_2$O and D$_2$O have been acquired. The spectra of the parallel-stranded DNA are then compared to the spectra of the antiparallel double helix formed from the deoxyoligonucleotides D1 and 5′-d(AAATATTTAAAATTA-(T)$_{10}$]-3′ (D3). The Raman spectra of the antiparallel-stranded (aps) duplex are reminiscent of the spectra of poly[d(A)]·poly[d(T)] and a B-form structure similar to that adopted by the homopolymer duplex is assigned to the antiparallel double helix. The spectra of the parallel-stranded (ps) and antiparallel-stranded duplexes differ significantly due to changes in helical organization, i.e., base pairing, base stacking, and backbone conformation. Large changes observed in the carbonyl stretching region (1600–1700 cm^{-1}) implicate the involvement of the C(2) carbonyl of thymine in base pairing. The interaction of adenine with the C(2) carbonyl of thymine is consistent with formation of reverse Watson–Crick base pairing in parallel-stranded DNA. Phosphate–furanose vibrations similar to those observed for B-form DNA of heterogenous sequence and high A,T content are observed at 843 and 1092 cm^{-1} in the spectra of the parallel-stranded duplex. The 843-cm^{-1} band is due to the presence of a sizable population of furanose rings in the C2′-endo conformation. Significant changes observed in the regions from 1150 to 1250 cm^{-1} and from 1340 to 1400 cm^{-1} in the spectra of the parallel-stranded duplex are attributed to variations in backbone torsional and glycosidic angles and base stacking.

The familiar A, B, and Z conformations of DNA are characterized by Watson–Crick base pairing between antiparallel oriented sugar–phosphate strands. Under a number of circumstances such as protonation at low pH, the introduction of bulky base substituents, triple- or quadruple-helix formation, and chemical modification of the backbone or glycosidic linkages, parallel-stranded (ps) structures can be formed [see Saenger (1984, Chapter 13) and van de Sande et al. (1988) for review and references]. The formation of parallel-stranded DNA at neutral pH was first shown (van de Sande et al., 1988) to occur in DNA hairpin structures of the sequence 3′-d[(A)$_{10}$-C-C-C-C-5′-5′-(T)$_{10}$]-3′ and 5′-d-[(A)$_{10}$-G-G-G-G-3′-3′-d(T)$_{10}$]-5′, where a single linkage in the hairpin is replaced by a 3′–3′ (or 5′–5′) internucleotide bond to assure that the d(A)$_{10}$d(T)$_{10}$ stems are in a parallel orientation. Parallel-stranded structures can occur in linear sequences if antiparallel-stranded (aps) structures are prohibited or made unfavorable due to sequence incompatibility (Ramsing & Jovin, 1988; Ramsing et al., 1989; Rippe et al., 1989). In general, parallel-strand formation can occur in sequences that allow for the formation of a significantly greater number of base pairs in the parallel than in the antiparallel orientation (Ramsing & Jovin, 1988).

Parallel-stranded DNA differs from antiparallel-stranded DNA with regard to susceptibility to chemical modification, enzymatic recognition, and electrophoretic, spectroscopic, and thermodynamic properties. For example, the electrophoretic mobility of ps-DNA is about 5% higher than the mobility of

aps-DNA (van de Sande et al., 1988; Ramsing & Jovin, 1988; Germann et al., 1988; Rippe et al., 1989). The ultraviolet absorption maximum of ps-DNA lies to slightly shorter wavelengths (blue shifted) relative to aps-DNA. For both ps- and aps-DNA, thermal denaturation produces a hypochromic increase in ultraviolet absorption. Analysis of the thermodynamic properties of parallel-stranded DNA indicates that the parallel-stranded duplex undergoes a cooperative thermal transition from a stacked to an unstacked state with a transition midpoint 10–18 °C lower than that of the corresponding antiparallel-stranded duplex (Ramsing et al., 1989; Rippe et al., 1989). The difference in the relative stability of antiparallel and parallel structures is reduced by the presence of divalent magnesium. Parallel and antiparallel DNA exhibit different susceptibilities to chemical modification (van de Sande et al., 1988; Rippe & Jovin, 1989; Klysik, Rippe, and Jovin, unpublished data). The drugs bis(benzimidazole) Hoechst-33258 (BBI-258) and 4′,6-diamidino-2-phenylindole dihydrochloride hydrate (DAPI), which bind selectively to the minor groove in B-DNA, have little affinity for ps-DNA, while the intercalator ethidium bromide exhibits a higher fluorescence quantum yield upon binding to ps than to aps duplexes (van de Sande et al., 1988; Ramsing & Jovin, 1988; Germann et al., 1989; Jovin et al., 1990). In addition to differences in chemical reactivity, parallel- and antiparallel-stranded duplexes differ in activity to various DNA processing enzymes (Rippe & Jovin, 1989). Parallel-stranded duplexes are not cut by restriction endonucleases *Dra*I, *Ssp*I, and *Mse*I. In contrast, ps-DNA exhibits a higher S1 nuclease activity but lower DNase I and exonuclease III activities than antiparallel DNA. Together these physicochemical and biochemical studies demonstrate that stable parallel-stranded duplexes are spectroscopically, chemically, and structurally distinct from their antiparallel-stranded counterparts.

[‡]Permanent address: Twente University of Technology, Department of Applied Physics, P.O. Box 217, 7500 AE Enshede, The Netherlands.
[§]University of Oregon.
[∥]Max Planck Institute.

Currently, direct conformation of the structure of ps-DNA by crystallographic techniques is not available and structural details of the helical organization of ps-DNA are limited. Model building provides a picture of ps-DNA with reverse Watson–Crick base pairing and the presence of two almost equivalent grooves along the helix such that the distinction between the major and minor grooves of aps-DNA is eliminated. Experimental verification of this model by ^{31}P and ^{1}H NMR is preliminary (Germann et al., 1989; Jovin et al., 1990).

The acquisition of a set of structural parameters for ps-DNA is critical to understanding the structural basis underlying the distinct chemical and spectroscopic properties of parallel-stranded DNA. To pursue this goal, the oligonucleotides D1, D2, and D3 were synthesized and hybridized to form the following ps and aps duplexes:

APS, D1·D3:

```
5'- A A A A A A A A A A T A A T T T T A A A T A T T T - 3'   (D1)
3'- T T T T T T T T T T A T T A A A A T T T A T A A A - 5'   (D3)
```

PS, D1·D2:

```
5'- A A A A A A A A A A T A A T T T T A A A T A T T T - 3'   (D1)
5'- T T T T T T T T T T A T T A A A A T T T A T A A A - 3'   (D2)
```

One strand (D1) is common to both duplexes but the second strands (D2, D3) are inverted sequences of one another. The oligonucleotides form a set of parallel and antiparallel duplexes of identical base composition. These sequences were selected because they are perfectly complementary in the desired orientations, either parallel (D1·D2) or antiparallel (D1·D3), but are poorly matched in all possible alternative potentially competitive homo- and heteroduplexed orientations. The $A_{10}\cdot T_{10}$ tract serves to eliminate potential alternative orientations, while the remaining 15-base tract defines the orientation of the duplex. Competition between hetero- and homoduplexes would be significant for oligomers containing the 15-base sequence alone. The vibrational properties of the ps and aps duplexes D1·D2 and D1·D3, were investigated by Raman spectroscopy. Analysis of the vibrational data provides for both the parallel and antiparallel duplexes structural details concerning base pairing, base stacking, furanose conformation, and backbone conformation. Exclusively adenine- and thymine-containing oligomers were chosen to simplify the characterization of the ps and aps duplexes. Analysis of oligomers containing cytosine and guanine (Rippe et al., 1990) will be a subject of future investigation. The absorption, thermodynamic, and physiochemical properties of the ps and aps duplexes, D1·D2 and D1·D3, and related duplexes have been characterized extensively (Rippe et al., 1989; Rippe & Jovin, 1989; Ramising et al., 1989; Jovin et al., 1990).

MATERIALS AND METHODS

The oligonucleotides were synthesized by conventional phosphoramidite chemistry with an Applied Biosystems Model 381A DNA Synthesizer (University of Oregon Biotechnology Laboratory). Following trityl group removal, the oligonucleotides were purified by reverse-phase HPLC on a Vydac C4 10-mm by 250-mm column. The oligomers were eluted with an acetonitrile versus 0.1 M trimethylamine acetate, pH 6.5, gradient. The purified fraction was concentrated to dryness by rotary evaporation. Oligonucleotides were desalted by repeated washing and centrifugation through Centricon 3 (Amicon Inc.) filters. Equimolar amounts of the single strands were mixed. The single-strand mixture was annealed at 54 °C for 5 min and allowed to cool slowly overnight to ensure complete duplex formation. Solution samples contained 20 mM sodium cacodylate, 100 mM NaCl, and 1 mM Na-EDTA

with a pH of 7.2. Samples in D_2O were obtained by lyophilizing the double-stranded molecules twice from D_2O to eliminate residual H_2O. Storage at low temperatures prevented the exchange of C8 protons. The Raman equipment consists of a Spectra Physics Model 2025 argon ion laser, a Spex spectrometer, a ITT 4013 UVG photomultiplier tube, and standard photon counting electronics. A 5-μL sample of each oligonucleotide solution was placed in a Kimax capillary tube and sealed. Capillary tubes were placed in a cell holder thermostated to 5 °C. About 50 scans from 500 to 1800 cm^{-1} were acquired for each sample. The C–H stretching region from 2800 to 3200 cm^{-1} was also recorded for the samples in D_2O. Spectra were recorded at a slit setting corresponding to a full-width band-pass of 3 cm^{-1}. Data manipulation was performed on a Hewlett-Packard 9836 computer. The experimental spectra presented have not been smoothed. A peak fit procedure combined with a method to also retrieve very weak bands (C. Otto, G. A. Thomas, and W. L. Peticolas, unpublished results) was used to analyze the data. This procedure enables a close comparison of the experimental data with theoretical data. Difference spectra were constructed by normalization of the spectra to both the 608-cm^{-1} cacodylate band of the buffer and the PO_2 vibration at 1092 cm^{-1}. Normalization to either band leads to the same result. Normal mode calculations have been performed for antiparallel-stranded DNA (Letellier et al., 1987a–d, 1989). The calculated band positions are presented in Table I. Normal mode calculations for parallel-stranded DNA have not been reported, so that the assignment of bands in the parallel-stranded spectrum must be considered tentative.

The spectra in Figure 2 were fit to a sum of Lorentzian bands by using a very carefully derived basis set of bands, and the fitting in this case is not arbitrary. The starting basis set includes bands that are directly observed in oligomers and in polymers containing the bases A and T as well as in model mononucleotides. They have been calculated by Letellier et al. (1987a–d, 1989), but the calculated frequencies are in agreement with IR and Raman measurements so that they present an experimentally observed as well as calculated basis set. Great care is taken to minimize the number of bands included to ensure that the procedure is not overdetermined. The uniqueness of the fit is carefully evaluated by examination of related fits that differ by the inclusion or exclusion of one or two bands. In general the procedure is a method of data analysis and is a way of looking at the data. The only real data are the spectra themselves. What is remarkable in our treatment is the extraordinary low signal-to-noise ratio in the flat baseline that results from the subtraction of the calculated spectrum from the experimental spectrum (see Figure 2). It is found that attempts to exclude or include an extra band leads to a considerable deterioration in the flatness and lack of noise of this difference spectrum. This gives us confidence in the validity of the numerous small bands that show up in the curve-resolved spectrum. The fact that these bands also agree with the normal mode calculations is also very encouraging.

RESULTS AND DISCUSSION

Both parallel and antiparallel double-stranded duplexes contain a large 10-base paired homo(A,T) tract followed by short fragmented homo(A,T) sections. To a first approximation, due to the nature of the sequence, the aps oligomer can be expected to possess similar conformational and spectroscopic properties as antiparallel poly[d(A)]·poly[d(T)]. Indeed, the Raman spectrum of the aps duplex displayed in Figure 1A closely resembles that observed for poly[d(A)·poly[d(T)]. For example, both the polymer and the aps duplex

Table I: Positions and Assignments in the Raman Spectra of Antiparallel- and Parallel-Stranded DNA[a]

band (cm⁻¹)				band (cm⁻¹)			
aps	ps	calculated	assignments	aps	ps	calculated	assignments
502	503			1144	1146	1133	furanose in dT
530	533	533	Th W(C2O), W(C4O), W(N1Cm), W(C5Cm)		1170	1184	furanose in dT
565	565				1190	1192, 1188	furanose in 2'-dA; furanose in dT
618	623			1211	1209	1202	furanose in dT
660	660			1231	1229	1222, 1244	Th; furanose in 2'-dA
670	670	669	Th B(C2N3C4), B(N3C4C5), B(C2'C1'O1'), B(C1'O1'C4')	1255	1254	1264, 1255	Th; furanose in 2'-dA; furanose in dT
729	730	727	Ad S(C1'O1'), B(C1'O1'C4'), S(C5N7), S(C6N6), S(C4C5), S(C4N3), S(C8N7), S(N3C2), S(C4N9)	1304	1306	1306	Ad
				1334	1335		Ad B(NC8H), B(NC2H), S(C2N3) (C3'-endo)
751	751		thymine-furanose, adenine–glycosidic bond stretch	1344	1345	1343	Ad B(NC8H), B(NC2H), S(C2N3) (C2'-endo)
789	789	773	thymine–furanose		1351		
796	793	788	phosphate–furanose backbone S(PO5'), S(P=O), B(C4'C3'H), B(C4'C5'O5')	1373	1376	1374	Ad S(C1'N9), S(C6N6)
		799	Ad T(C2N1), T(C2N3), W(C2H)	1378	1381	1370	Th CH₃-sym def, S(C2N3), S(C5CH3), S(N1C6)
816	801–805	813	furanose in 2'-dA; C3'-endo furanose–backbone	1388	1388	1388	Th CH₃ sym def, S(C1'N1)
		825		1421	1422	1422	Ad S(C8N9), S(C1'N9)
843	843	821	phosphate–furanose backbone S(PO5'), B(C4'C5'H), S(C3'C4'), B(O5'C5'H); C2'-endo furanose–backbone	1444	1444	1443	Th CH₃ asym def
	876	864	furanose in 2'-dA; furanose in dT	1462	1462	1452	Ad S(N1C6), S(C6N6)
895	894	905, 886	Ad; furanose in dT	1482	1482	1470	Th S(C4C5), S(N1C2)
928	924	925, 919	furanose in 2'-dA; furanose in dT	1488	1488	1491	Ad B(NC8H), S(N7C8), S(C2N3), S(N3C4)
973	976	976, 958	furanose in 2'-dA; furanose in dT	1513	1512	1508	Ad B(NC2H), S(C2N3), S(N1C2), S(C5C6)
	1005				1536		
1015	1018	1026, 1022	furanose in 2'-dA; furanose in dT	1578	1581	1578	Ad S(C5C6), S(C4C5), S(C5N7)
1055	1054	1050	furanose in dT	1660	1659	1649, 1651	Th S(C5C6), S(C4O4); Ad HN6H, S(C6N6), B(C6N6H)
1076	1072	1084	furanose in dT	1667	1670	1686	Th S(C4O4), S(C2O2), S(C5C6)
1092	1094		(O=P=O) in-phase stretch vib	1667	1682	1756	Th S(C2O2), S(C4O4)
1112	1115	1113	furanose in dT	2893	2893		S(CH) deoxyribose–phosphate
				2935	2935		S(CH) methyl group thymine
				2954	2954		S(CH) deoxyribose–phosphate
				2980	2980		S(CH) deoxyribose–phosphate
				3016	3016		S(C8H) adenine

[a] Band positions for antiparallel- and parallel-stranded duplexes are compared to calculated values obtained from normal mode analysis of thymidine, 2'-deoxyadenosine, and a model phosphate backbone in an antiparallel-stranded geometry (Letellier et al., 1987a,b, 1989). Abbreviations: Ad, adenine; Th, thymine; S, stretching mode; B, bending mode; W, wagging mode; T, torsional mode; (a)sym, (a)symmetric; def, deformation.

have well-defined prominent bands at 843 and 1092 cm⁻¹, along with a shoulder at 816 cm⁻¹ (Thomas & Peticolas, 1983). The band at 1092 cm⁻¹ is due to the symmetric vibration of the PO₂ group. In B-form DNA of heterogenous sequence this band appears at 1092–1095 cm⁻¹. In A-form DNA the band is observed at 1100 cm⁻¹ (Erfurth et al., 1975). The 843-cm⁻¹ band is due to the population of furanose rings in the C2'-endo conformation associated with classical uniform B-form DNA. The 816-cm⁻¹ band was previously assigned, in the case of poly[d(A)]·poly[d(T)], to a small but defined population of furanose rings in the C3'-endo conformation. The C3'-endo conformation is usually associated with classical uniform A-form DNA. The native B-form of DNA is somewhat heterogenous with regard to furanose conformation, and inclusion of a small population of furanose rings in the C3'-endo conformation in a B-form helix has been observed for other oligomers (Kubasek et al., 1986; Wang et al., 1987; Peticolas et al., 1989; Wartell, 1987). In the case of poly[d-(A)·poly[d(T)], the small C3'-endo furanose population was believed to reside primarily in the adenine strand of the duplex. Consistent with this, coupled vibrations involving adenine attached to C2'-endo and C3'-endo sugars have been observed for the polymer at 1344 and 1334 cm⁻¹, respectively (Katahira et al., 1986; Taillandier et al., 1987). For the aps duplex, the 816-, 843-, 1334-, and 1344-cm⁻¹ bands can be observed in the spectrum displayed in Figure 1A and in the curve-resolved spectra displayed in Figure 2A,B. The spectrum of the aps duplex is also similar to the spectrum of the alternating co-

polymer poly(dA-dT) (Thomas & Peticolas, 1983; Small & Peticolas, 1971; Jenkins et al., 1986). Detailed band assignments for both the aps and ps duplexes based upon theoretically calculated band positions obtained from recent normal mode calculations on thymidine, 2-deoxyadenosine, and the phosphate–sugar backbone are contained in Table I. The data suggest that a somewhat heterogeneous B-form conformation similar to that observed for poly[d(A)·poly[d(T)] is adopted by the aps duplex in solution.

Though the ps duplex also contains a large homo(A,T) stretch, the Raman spectrum of this duplex displayed in Figure 1B differs substantially from the spectrum of the corresponding aps duplex, implying that the two duplexes differ conformationally. Similar to the case of aps-DNA, bands at 843 and 1092 cm⁻¹ are observed in the spectrum of the ps duplex. These two bands are usually observed in the spectra of B-form DNA and are usually taken as diagnostic for the presence of a B-form helix. Formally, the 843-cm⁻¹ band, as discussed above, provides a measure of the population of furanose rings in the C2'-endo conformation and not B-form helicity. The intensity of the 843-cm⁻¹ band indicates that a sizable population of furanose rings in the C2'-endo conformation are present in the ps duplex. The presence of furanose rings in the C2'-endo conformation has also been detected by two-dimensional NMR (Germann et al., 1989). In the case of the ps duplex the presence of the two bands may indicate the preservation of basic elements of B-form helix even though the B-form helix is formally described only for antiparallel
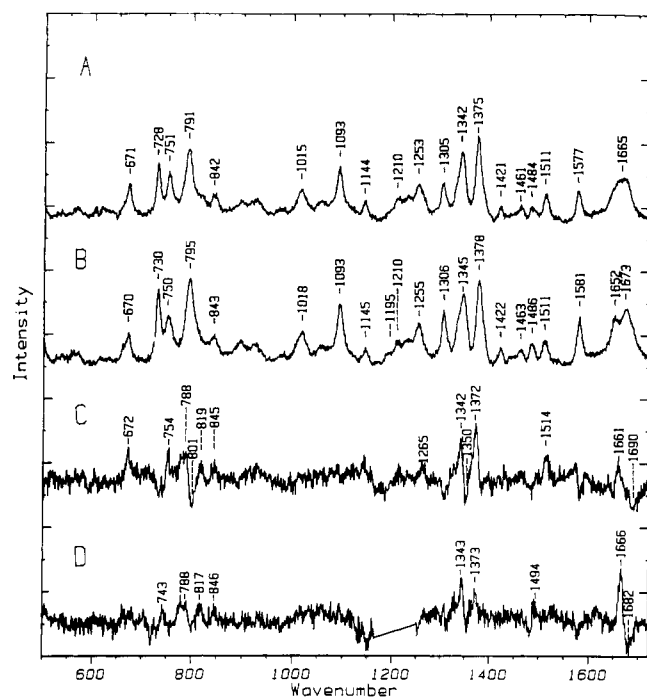
FIGURE 1: Raman spectrum of antiparallel-stranded DNA (A) and parallel-stranded DNA (B) in H₂O. Water contributions have been removed from (A) and (B) by subtraction. The indicated peak positions are maxima in the spectrum. Figure 1C contains the difference spectrum of antiparallel-stranded minus parallel-stranded DNA in H₂O. Figure 1D is the difference spectrum obtained in D₂O. The region in (D) where the bending mode of D₂O strongly contributes is replaced by a straight line for the sake of clarity. The vertical scale of the difference spectra is expanded by a factor of 2 with respect to the original spectra. All spectra have not been smoothed.

double strands. Beyond this similarity, the spectra of the ps and aps duplexes differ significantly in the regions 650–850, 1300–1400, and 1600–1700 cm^{-1}. Intensity and frequency changes in these regions can be observed by examination of the difference spectra contained in Figure 1C,D. The differences observed in the spectra of the ps and aps duplexes correspond to differences in furanose conformations, base stacking, and base pairing.

Analysis of the carbonyl region from 1600 to 1700 cm^{-1} for the ps and aps duplexes indicates that the base pairing in parallel-stranded DNA is most likely reverse Watson–Crick, that is, with the glycosyl bonds in the trans configuration. There are four accepted base-pairing schemes, which may be grouped into two classes that differ in involvement of either the C(2)=O or C(4)=O carbonyl of the pyrimidine base. Watson–Crick and Hoogsteen base pairing involve, in the case of adenine–thymine base pairs, interactions between A(N6H₂) and T(C4=O) and between A(N1) and T(N3H) (Watson–Crick) or between A(N6H₂) and T(C4=O) and between A(N7) and T(N3H) (Hoogsteen). The reverse Watson–Crick and Hoogsteen orientations involve hydrogen bonding to T-(C2=O) instead of T(C4=O) with the following interactions: A(N6H₂) with T(C2=O) and A(N1) with T(N3H) (reverse Watson–Crick) and A(N6H₂) with T(C2=O) and A(N7) with T(N3H) (reverse Hoogsteen) (see Figure 3). In ordinary Watson–Crick base pairing as well as in Hoogsteen base pairing the C4=O group participates in a hydrogen bond with adenine. Hoogsteen base pairing compared with Watson–Crick base pairing is not expected to give rise to large changes in the carbonyl stretching vibrations in the 1600–1700-cm^{-1} region. Examinations of Hoogsteen base pairing in cocrystals of 9-methyladenine and 1-methylthymine (Strobel & Scovell, 1980) and in triple-helical poly(A)·2 poly(U) (Kiser, 1975;

O'Connor & Bina, 1984) confirm this expectation. In reverse Watson–Crick and reverse Hoogsteen base pairing the C2=O group rather than the C4=O group participates in hydrogen bonding to adenine. In the case of adenine-thymine base pairs, reverse Watson–Crick and reverse Hoogsteen base pairing will generate a very different set of carbonyl vibrations compared to Watson–Crick and Hoogsteen base pairing. As a consequence, one expects to observe a very different spectrum in the carbonyl region for the reverse orientation compared to the normal orientation. In the case of the ps and aps duplexes, large differences between the spectra of these duplexes in the region from 1600 to 1700 cm^{-1} are expected only if base pairing in a reverse orientation involving the C(2) carbonyl is present in the ps duplex.

Consistent with a reverse orientation involving the thymine C2 carbonyl, large differences are observed in the spectra of ps and aps duplexes in the region from 1600 to 1700 cm^{-1} (Figure 1A–C). Specifically, a residual positive intensity at 1661 cm^{-1} and negative intensity at 1690 cm^{-1} is observed in the difference spectrum acquired in H₂O. Water contributes strongly to the region around 1635 cm^{-1}, potentially interfering with the carbonyl stretching region. This interference is avoided by using D₂O, where the 1635-cm^{-1} band is displaced to 1250 cm^{-1}. The difference spectrum acquired in D₂O (Figure 1D) is remarkably similar to the corresponding spectrum acquired in H₂O (Figure 1C). In D₂O a residual positive intensity is observed at 1666 cm^{-1} and a negative intensity at 1682 cm^{-1}. The region from 1600 to 1700 cm^{-1} can be examined in greater detail by inspection of Figure 4, which contains the results of a fit of the experimental data to a sum of Lorentzians. In Figure 4C the difference spectrum of the experimental curves is accurately reproduced by the difference spectrum of the calculated curves. In the case of the aps duplex, Lorentzian bands are calculated at 1660 and 1667 cm^{-1}. For the ps duplex, bands at 1659, 1670, and 1682 cm^{-1} are required to adequately represent the experimental data. A very different set of carbonyl vibrations is observed for the ps duplex compared to the aps duplex. The data within the 1600–1700-cm^{-1} region is consistent with involvement of the C(2) carbonyl in reverse Watson–Crick or reverse Hoogsteen base pairing. The possibility of reverse Hoogsteen base pairing can be eliminated by examination of selected vibrations of adenine.

In Hoogsteen base pairing the external amino group and the N7 atom of adenine are involved in hydrogen bonding to the complementary thymine base. In Watson–Crick base pairing the external amino group and the N1 atom of adenine are involved in hydrogen bonding. The occurrence of reverse Hoogsteen base pairing will result in characteristic differences in the carbonyl stretching region as well as in bands due to the adenine molecule. One of the largest changes in the Raman scattering of the adenine residue observed as a result of Hoogsteen base pairing is a large decrease in the intensity of the 1421-cm^{-1} band. In a study (Thomas & Peticolas, 1983) of the formation of triple-helical poly(dT)·poly(dA)·poly(dT), the 1421-cm^{-1} band was observed to decrease upon addition of the second poly(dT) strand. The second poly(dT) strand is Hoogsteen base-paired to the double-helical Watson–Crick base-paired poly(dA)·poly(dT). In a recent ultraviolet resonance Raman study (Grygon et al., 1989) of triple-stranded helices of poly(U·A·U), interaction at the N(7) position was identified by a decrease in the intensity of the 1344- and 1482-cm^{-1} bands, in analogy to changes in guanine vibrations when positively charged ions interact with the N(7) position. In contrast, an increase in the intensity of the 1480-cm^{-1} band
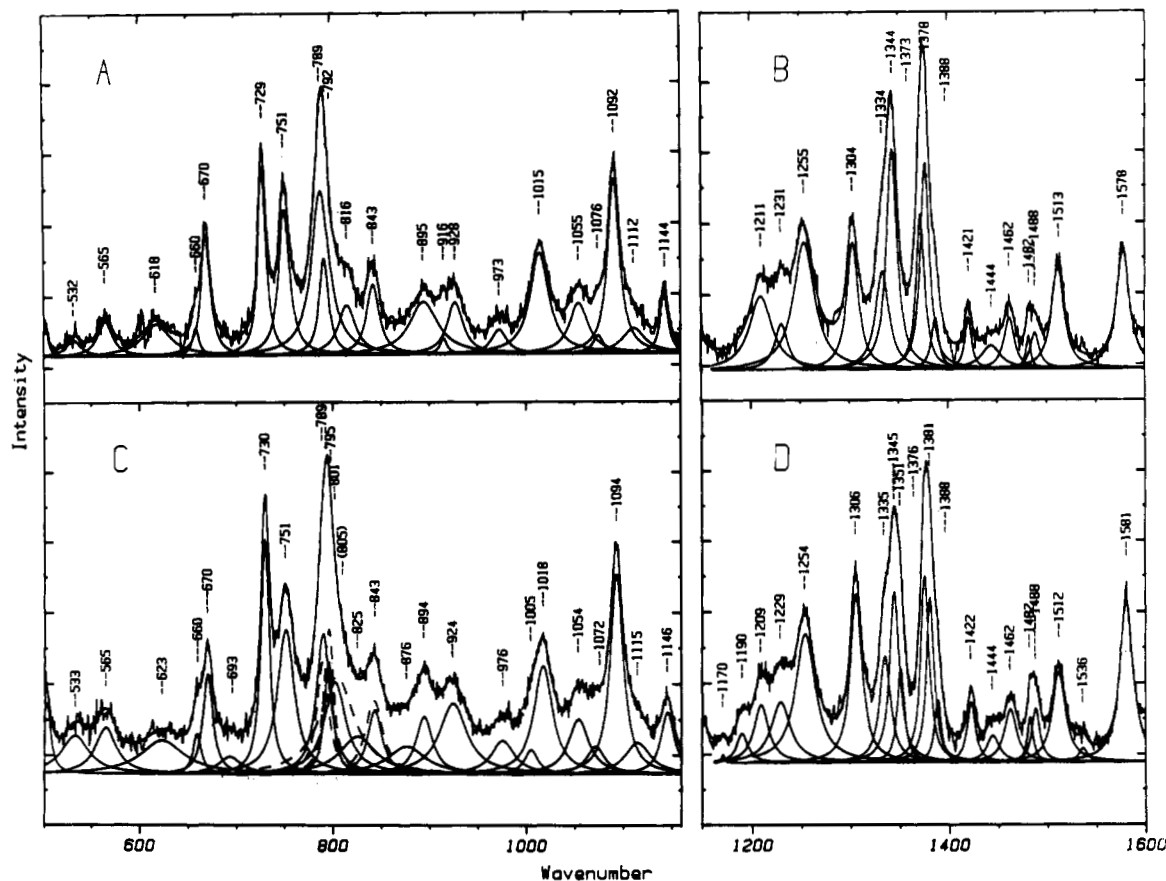
FIGURE 2: Results of a fit of the experimental data to set of Lorentzian bands. The experimental curves, calculated curves, and individual Lorentzian components are displayed. The upper plots (A and B) correspond to the antiparallel duplex. Data for the parallel duplex are displayed in the lower plots (C and D). The dashed components in (C) are Lorentzian contributions to an alternative fit where the 801- and 825-cm^{-1} bands have been replaced by a single band at 805 cm^{-1}. The label for this band appears in parentheses. The label for the 1388-cm^{-1} band appears at 1400 cm^{-1} to avoid overlap between the label and the data.
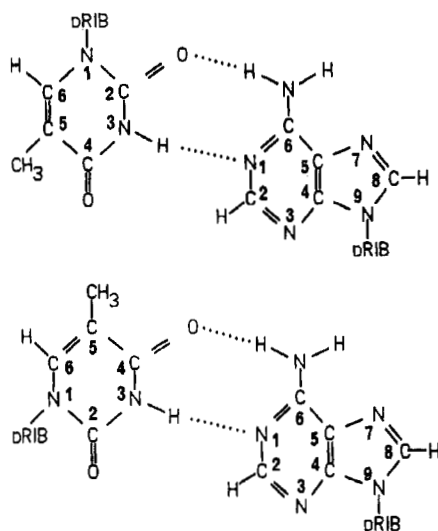
FIGURE 3: Base pairing in reverse Watson–Crick (A) and Watson–Crick (B) orientations.

and little change in the 1421-cm^{-1} band were observed in the spectrum of the parallel-stranded duplex. These observations are inconsistent with base pairing involving the N(7) position of adenine. The large differences in the spectra of the ps and aps oligomers in the region from 1600 to 1700 cm^{-1} in conjunction with the lack of evidence supporting involvement of the N(7) position leads to the conclusion that the base pairing in parallel-stranded DNA is reverse Watson–Crick.

Comparison of the spectra of the ps and aps duplexes in the regions 650–750 and 1200–1400 cm^{-1} indicates that the base

stacking and chemical environment of the C(5) thymine methyl group within the parallel and antiparallel helices differ. The intensities of the bands at 672 (T), 754 (T), 1342 (A), and 1378 (A,T) cm^{-1} are greater in the spectrum of the antiparallel-stranded duplex than in that of the parallel-stranded duplex (Figure 1A,B). As a result, positive contributions at these positions are observed in the difference spectrum displayed in Figure 1C. Reduction in band intensity at 672 and 754 cm^{-1} accompanies thermal denaturation and formation of an A-form helix for A,T-containing copolymers. In addition, adoption of an A-form helix is accompanied by an apparent splitting of the 672-cm^{-1} band into two components, 666 and 642 cm^{-1}, and a shift in the 754-cm^{-1} band to 747 cm^{-1}. The reduced intensity at 672 and 754 cm^{-1} and the lack of shifts in the position of these bands in the spectrum of the ps duplex are consistent with a reduction in base–base overlap and/or orientation, similar to but not to the extent encountered in helical unwinding or thermal denaturation. The fact that both of these bands arise from thymine suggests that pyrimidine-pyrimidine base pairs may be affected to a greater degree.

The 1378-cm^{-1} band contains multiple contributions from both thymine and adenine. This broad structure in both the ps and aps duplex spectra can be decomposed into three Lorentzian components (Figure 2B,D). The relative intensity of the three components differ in the spectra of the parallel- and antiparallel-stranded DNA (Figure 2C,D). Assignment of particular components exclusively to either adenine or thymine is difficult. The change in intensity of the three components is reminiscent of hypo- and hyperchromic spectral changes that accompany changes in base stacking, i.e., overlap or orientation. This suggests that adoption of a parallel-
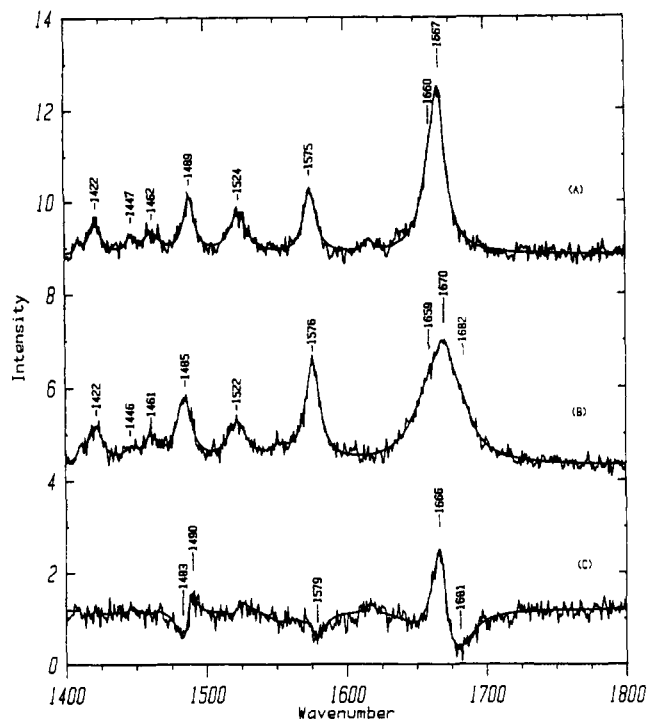
FIGURE 4: Carbonyl stretching mode region of the spectrum of antiparallel-stranded DNA (A) and parallel-stranded DNA (B) in a D_2O solution. The difference spectrum (antiparallel DNA – parallel DNA) is contained in(C). The difference spectrum is on the same scale as the original spectra. The smooth curve is obtained from a fit of the data to a sum of Lorentzians.

stranded structure involves alterations in base-stacking interactions. This suggestion is consistent with a molecular dynamics model in which optimization of the structure results in a rough equivalence of the two grooves of ps-DNA, which necessarily implies different pyr-pyr and pur-pur stacking in the ps helix compared to the aps helix (van de Sande et al., 1988). On the basis of this model, one would anticipate that perturbations due to changes in base stacking would be observed in the spectrum of the parallel-stranded DNA.

The band at 1343 cm^{-1} is due to adenine. A decrease in intensity is observed for the ps oligomer compared to the aps oligomer, but no shift in frequency is observed. The intensity difference at 1343 cm^{-1} appears to arise from hypochromic intensity changes due to realignment of purine base stacking.

In addition to the spectral differences in the 1300–1400-cm^{-1} region noted above, a negative band at 1351 cm^{-1} is observed in the difference spectrum displayed in Figure 1C. This band is present in the difference spectrum recorded in D_2O (Figure 1D) and is also readily identified in the calculated spectrum (Figure 2D). The assignment of this band in the spectrum of the parallel-stranded duplex is unclear. The presence of the 1351-cm^{-1} band can be detected in the difference spectrum of the antiparallel- and parallel-stranded DNA obtained in D_2O (Figure 1D). Since samples were stored and measured at low temperatures where exchange of the C(8) protons is negligible, only the "acidic" protons on the nitrogen atoms of the bases undergo deuterium exchange. If the C8 proton is substituted for a deuteron then the 1485–1489-cm^{-1} band shifts to 1460 cm^{-1} (Benevides & Thomas, 1985). The presence of a band at 1489 cm^{-1} in the spectrum of the aps duplex (1485 cm^{-1} in ps duplex) indicates that deuterium exchange at the C(8) position has not occurred. The 1351-cm^{-1} band in the spectrum of the ps duplex does not respond to deuterium exchange involving the "acidic" protons on the nitrogen atoms of the bases. The vibration at 1351 cm^{-1} may be a base–

furanose vibration analogous to the coupled sugar–adenine vibration at 1334 cm^{-1} (C3′-endo) and 1344 cm^{-1} (C2′-endo) but involving a very different sugar conformation. In the difference spectrum constructed from the spectrum of poly-[d(A-T)] in the B and A conformations, a negative band at 1351 cm^{-1} is not observed (Prescott et al., 1984). Therefore, the 1351-cm^{-1} band may be characteristic for and unique to the structure of parallel-stranded DNA.

In spite of the relative ease of adoption of a parallel-stranded duplex, significant alterations in the furanose–phosphate backbone, including changes in the distribution of furanose ring conformations, accompany formation of a stable parallel-stranded structure. In the difference spectrum displayed in Figure 1C, small positive contributions at 788, 819, and 845 cm^{-1} along with a strong negative contribution at 801 cm^{-1} are observed. In Figure 2A, which contains a fit of the experimental data to a sum of Lorentzians, four bands at 788, 792, 816, and 843 cm^{-1} are identified. The 816- and 843-cm^{-1} bands, as described previously, are assigned to the populations of furanose rings in the C3′-endo and C2′-endo conformations, respectively. The region from 775 to 850 cm^{-1} of the spectrum of the ps duplex can also be fit with four bands at 788, 795, 806, and 843 cm^{-1} (Figure 2B). The 843-cm^{-1} band does not differ greatly in the spectra of the ps and aps helices. The band at 806 cm^{-1} in the spectrum of the ps duplex is exceptionally broad with a half-width of approximately 22 wavenumbers. The position and breadth of this band suggest that a broad distribution of furanose conformations perhaps closely related to the C3′-endo conformation may be present in the parallel-stranded DNA. The breadth of this band is of concern and may mask the presence of unresolved contributions. The experimental spectrum of the ps duplex can be fit with an additional band in this region. In this case, bands are identified by the fitting procedure at 789, 795, 801, 827, and 843 cm^{-1}. Both bands at 801 and 827 cm^{-1} are fairly broad with half-widths of 16 and 18 cm^{-1}, respectively. Neither band can be assigned with a large degree of certainty. The 827-cm^{-1} band may arise from furanose conformations intermediate between the C3′-endo and C2′-endo, such as the O1′-endo. The two sets of fitting parameters generate fits to the experimental data of comparable adequacy. In either case, the 800–820-cm^{-1} region in the spectrum of the ps duplex differs drastically from the corresponding region in the spectrum of the aps duplex. On the basis of the observations described above, one may reasonably conclude that parallel-stranded DNA contains a large degree of furanose conformational and structural heterogeneity along with a significant amount of furanose rings in the C2′-endo conformation. This conclusion is supported by ^{31}P NMR data concerning the same two ps and aps duplexes in which a broadening of the spectrum of the former compared to the latter is observed (Jovin et al., 1990).

Two bands at 1170 and 1190 cm^{-1} are present in the spectrum of the ps duplex and not in the spectrum of the aps duplex. The 1170-cm^{-1} band is assigned to a furanose vibration of thymidine. The 1190-cm^{-1} band contains contributions from both 2′-deoxyadenosine and thymidine furanose rings. The bands are not observed in B-form DNA and appear to be unique to the parallel structure.

Differences in backbone geometry and furanose conformation between the ps and aps structures can also be identified by examination of the C–H stretching region from 2800 to 3200 cm^{-1}. Spectra of the ps and aps duplexes from 2800 to 3200 cm^{-1} are displayed in Figure 5. The spectra were obtained in D_2O to minimize contributions from the strong H_2O spectrum in this region. The 2800–3200-cm^{-1} region contains
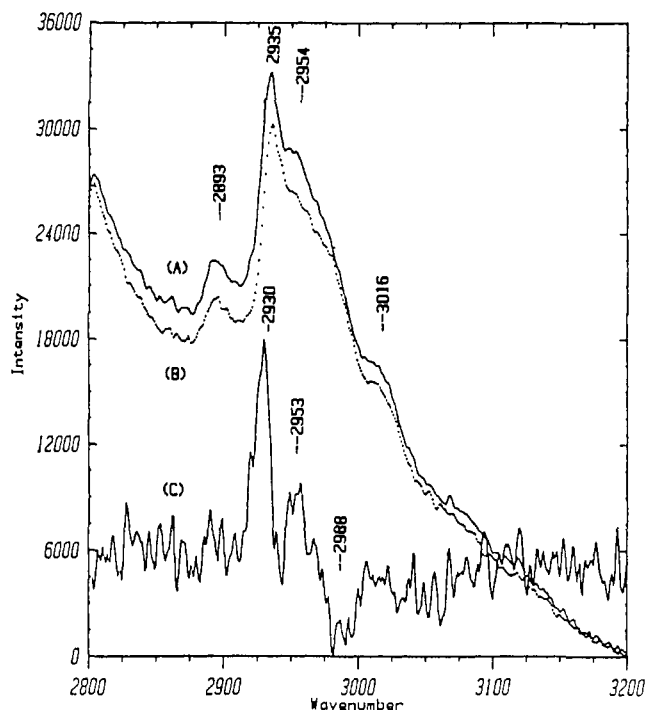
FIGURE 5: C–H stretching region of antiparallel stranded DNA (A) and parallel-stranded DNA (B) in D_2O. The difference spectrum (C) is on the same scale.

the C–H stretch vibrations of the sugar groups, the C2–H and C8–H stretch of the adenine residues, and the methyl C–H stretch vibrations of the thymine residues. Two positive bands at 2930 and 2953 cm^{-1} and a negative band at 2988 cm^{-1} are identified in the difference spectrum in Figure 5. The aromatic C–H stretch vibrations can be observed as weak vibrations around 3064 cm^{-1}. The methyl group vibrations of the thymine residue contribute at 2935 cm^{-1} together with the C–H stretch vibrations of the furanose ring (Prescott et al., 1984). The change in the band around 2935 cm^{-1} is may be attributed to repositioning of the methyl group with respect to the grooves of ps-DNA (Rippe & Jovin, 1989; van de Sande et al., 1988; Pattabiraman, 1986). The positive and negative components observed at 2953 and 2988 cm^{-1}, respectively, can be assigned to differences in furanose vibrations between the two structures.

CONCLUSIONS

In this paper the results of the first Raman spectroscopic study of a parallel-stranded 25-base-pair stretch of DNA are described. The difference spectra of (antiparallel DNA minus parallel DNA in both H_2O and D_2O contain corresponding positive and negative peaks. Large changes in the carbonyl stretching region from 1600 to 1700 cm^{-1} and the absence of changes characteristic for Hoogsteen base pairing are consistent with reverse Watson–Crick base pairing in the parallel-stranded oligomer. Analysis of the spectroscopic differences between the ps and aps duplexes suggests that changes in base stacking, i.e., base overlap and orientation, occur concomitantly with and may be necessary for adoption of a parallel-stranded structure. Analysis of the region from 750 to 850 cm1–^{1} indicates that the parallel-stranded structure is quite heterogeneous with regard to furanose conformation. Three bands unique to the structure of parallel-stranded DNA appear at 1162, 1189, and 1351 cm^{-1}. A more precise interpretation of the differences observed between the spectra of the ps and aps oligomers and an assessment of the geometrical changes that underlie them must await the calculation of the normal modes of parallel-stranded DNA.

REFERENCES

Arnott, S., Smith, P. J. C., & Chandrasekaran, R. (1976) *CRC Handbook of Biochemistry and Molecular Biology* (Fasman, G. D., Ed.) 3rd ed., Vol. 2, CRC Press, Cleveland, OH.
Benevides, J. M., & Thomas, G. J., Jr. (1983) *Nucleic Acids Res. 11*, 5747–5761.
Benevides, J. M., & Thomas, G. J., Jr. (1985) *Biopolymers 24*, 667–682.
Erfurth, S. C., Kiser, E. J., & Peticolas, W. L. (1972) *Proc. Natl. Acad. Sci. U.S.A. 69*, 938–941.
Germann, M. W., Kalisch, B. W., & van de Sande, J. H. (1988) *Biochemistry 27*, 8302–8306.
Germann, M. W., Vogel, H. J., Pon, R. T., & van de Sande, J. H. (1989) *Biochemistry 28*, 6220–6228.
Grygon, C. A., Davis, D. F., Spiro, T. G., & Fresco, J. R. (1991) *Proc. Natl. Acad. Sci. U.S.A.* (in press).
Jenkins, B. G., Wartell, R. M., & Alderfer, J. L. (1986) *Biopolymers 25*, 823–849.
Jovin, T. M., Rippe, K., Ramsing, N. B., Kelement, R., Elhorst, W., & Vojtiskovz, M. (1990) in *Biological Structures, Dynamics, Interactions & Expression*, Proceedings of the 6th Conservation in Biomolecular Stereodynamics (Sarma, R., & Sarma, M. H., Eds.) Vol. 2, Adenine Press, Guilderland, NJ (in press).
Kiser, E. J. (1975) Ph.D. Dissertation, University of Oregon, Eugene, OR.
Kubasek, W. L., Wang, Y., Thomas, G. A., Patapoff, T. W., Schoenwaelder, K.-H., Van der Sande, J. H., & Peticolas, W. L. (1986) *Biochemistry 25*, 7440–7445.
Letellier, R., Ghomi, M., & Taillandier, E. (1987a) *Eur. Biophys. J. 14*, 227–241.
Letellier, R., Ghomi, M., & Taillandier, E. (1987b) *Eur. Biophys. J. 14*, 243–252.
Letellier, R., Ghomi, M., & Taillandier, E. (1987c) *Eur. Biophys. J. 14*, 423–430.
Letellier, R., Ghomi, M., & Taillandier, E. (1987d) *J. Biomol. Struct. Dyn. 4*, 663–683.
Letellier, R., Ghomi, M., & Taillandier, E. (1989) *J. Biomol. Struct. Dyn. 6*, 755–768.
O'Connor, T., & Bina, M. (1984) *J. Biomol. Struct. Dyn. 2*, 615–625.
Pattabiraman, N. (1986) *Biopolymers 25*, 1603–1606.
Peticolas, W. L., Thomas, G. A., & Wang, Y. (1989) *J. Mol. Liq. 41*, 367–388.
Prescott, B., Steinmetz, W., & Thomas, G. J., Jr. (1984) *Biopolymers 23*, 235–256.
Ramsing, N. B., & Jovin, T. M. (1988) *Nucleic Acids Res. 16*, 6659–6676.
Ramsing, N. B., Rippe, K., & Jovin, T. M. (1989) *Biochemistry 28*, 9528–9535.
Rippe, K., & Jovin, T. M. (1989) *Biochemistry 28*, 9542–9549.
Rippe, K., Ramsing, N. B., & Jovin, T. M. (1989) *Biochemistry 28*, 9536–9541.
Saenger, W. (1984) *Principles of Nucleic Acid Structure*, Springer-Verlag, New York.
Small, E. W., & Peticolas, W. L. (1971) *Biopolymers 10*, 1377–1416.
Strobel, J. L., & Scovell, W. M. (1980) *Biochim. Biophys. Acta 608*, 201–214.

Taillandier, E., Ridoux, J.-P., Liquier, J., Leupin, W., Denny, W. A., Wang, Y., Thomas, G. A., & Peticolas, W. L. (1987) *Biochemistry 26*, 3361–3368.

Thomas, G. A., & Peticolas, W. L. (1983) *J. Am. Chem. Soc. 105*, 993–996.

Thomas, G. A., & Peticolas, W. L. (1983) *J. Am. Chem. Soc. 105*, 993–996.

Thomas, G. J., Jr., & Benevides, J. M. (1985) *Biopolymers 24*, 1101–1105.

van de Sande, J. H., Ramsing, N. B., Germann, M. W., Elhorst, W., Kalisch, B. W., von Kitzing, E., Pon, R. T., Clegg, R. C., & Jovin, T. M. (1988) *Science 241*, 551–557.

Wang, Y., Thomas, G. A., & Peticolas, W. L. (1987) *J. Biomol. Struct. Dyn. 5*, 249–274.

Mechanism of Site-Specific DNA Damage Induced by Methylhydrazines in the Presence of Copper(II) or Manganese(III)[†]

Shosuke Kawanishi* and Koji Yamamoto

Department of Public Health, Faculty of Medicine, Kyoto University, Kyoto 606, Japan

Received October 16, 1990; Revised Manuscript Received December 14, 1990

ABSTRACT: DNA damage induced by methylhydrazines (monomethylhydrazine, 1,1-dimethylhydrazine, and 1,2-dimethylhydrazine) in the presence of metal ions was investigated by a DNA sequencing technique. 1,2-Dimethylhydrazine plus Mn(III) caused DNA cleavage at every nucleotide without marked site specificity. ESR–spin-trapping experiments showed that the hydroxyl free radical (•OH) is generated during the Mn(III)-catalyzed autoxidation of 1,2-dimethylhydrazine. DNA damage and •OH generation were inhibited by •OH scavengers and superoxide dismutase, but not by catalase. The results suggest that 1,2-dimethylhydrazine plus Mn(III) generates •OH, not via H_2O_2, and that •OH causes DNA damage. In the presence of Cu(II), DNA cleavage was caused by the three methylhydrazines frequently at thymine residues, especially of the GTC sequence. The order of Cu(II)-mediated DNA damage (1,2-dimethylhydrazine > monomethylhydrazine ~ 1,1-dimethylhydrazine) was not correlated with the order of methyl free radical (•CH₃) generation during Cu(II)-catalyzed autoxidation (monomethylhydrazine > 1,1-dimethylhydrazine ≫ 1,2-dimethylhydrazine). Catalase and bathocuproine, a Cu(I)-specific chelating agent, inhibited DNA damage while catalase did not inhibit the •CH₃ generation. The order of DNA damage was correlated with the order of ratio of H_2O_2 production to O_2 consumption observed during Cu(II)-catalyzed autoxidation of methylhydrazines. These results suggest that the Cu(I)–peroxide complex rather than the •CH₃ plays a more important role in methylhydrazine plus Cu(II)-induced DNA damage.

A number of hydrazine derivatives are found in nature and used in industry, agriculture, and medicine. Most of the hydrazine derivatives have been shown to be carcinogenic and/or mutagenic (Kimball, 1977; Toth, 1980; Parodi et al., 1981). Methylhydrazines such as 1,2-dimethylhydrazine, 1,1-dimethylhydrazine, and monomethylhydrazine are carcinogenic in the large bowel of rodents (Toth, 1977, 1980). It was reported that 1,2-dimethylhydrazine was 100 times more carcinogenic, producing tumors selectively in the colon, than 1,1-dimethylhydrazine (Druckrey et al., 1967; Baló, 1979). Although 1,2-dimethylhydrazine has been widely used for the study of colon cancer, its carcinogenic mechanism remains to be clarified. It has been proposed that 1,2-dimethylhydrazine is enzymatically metabolized to the proximate carcinogen (methylazoxy)methanol, which is further transformed to an ultimate carcinogen, methyldiazonium, that methylates DNA (Fiala, 1977). However, there are several papers against this hypothesis. Rogers and Pegg (1977) reported that since DNA was methylated to a much lesser extent in the colon than in the liver of rats treated with 1,2-dimethylhydrazine, factors other than the production of methylguanine must be important in the initiation of colon cancer. Recently, the participation

of the methyl free radical (•CH₃)[1] in 1,2-dimethylhydrazine-induced carcinogenesis has been suggested (Kang et al., 1988; Albano et al., 1989). Relevantly, Augusto et al. (1984) reported that DNA strand scission was caused by the carbon radical derived from 2-phenylethylhydrazine metabolism. In addition, metal was shown to enhance 1,2-dimethylhydrazine-induced sister-chromatid exchanges and unscheduled DNA synthesis in cultured cells (MacRae & Stich, 1979; Whiting & Wei, 1979), and nonenzymatic biotransformation of monomethylhydrazine and 1,1-dimethylhydrazine was reported (Godoy et al., 1983). Therefore, regarding the mechanism of carcinogenicity and mutagenicity of methylhydrazines, it can be speculated that methylhydrazines are activated nonenzymatically by endogenous substances, such as metal ions, to produce active species causing DNA damage.

In this study, the mechanism of DNA damage by methylhydrazines (monomethylhydrazine, 1,1-dimethylhydrazine, and 1,2-dimethylhydrazine) in the presence of metal ions was investigated by both the DNA sequencing technique and the ESR–spin-trapping method.

[1] Abbreviations: •CH₃, methyl free radical; DTPA, diethylenetriaminepentaacetic acid; SOD, superoxide dismutase; DMPO, 5,5-dimethyl-1-pyrroline *N*-oxide; •OH, hydroxyl free radical; DMPO–OH, •OH adduct of DMPO; DMPO–CH₃, •CH₃ adduct of DMPO; POBN, α-(1-oxo-4-pyridyl)-*N-tert*-butyl nitrone; POBN–CH₃, •CH₃ adduct of POBN; O_2^-, superoxide radical.